

Supporting Information for

**Emerging investigator series: Correlating of Phase Composition and
Geometric Structure to the Colloidal Stability of 2D MoS₂
Nanomaterials**

Bei Liu^{a#}, Zixin Han^{a#}, Qi Han^a, Yufei Shu^a, Mengxia Wang^a, Li Wang^a,
Zhongying Wang^{a*}, Joel A. Pedersen^b

^a School of Environmental Science and Engineering, Southern University of Science and
Technology, Shenzhen 518055, China

^b Department of Environmental Health and Engineering, Johns Hopkins University,
Baltimore, MD, 21218, United States

* to whom correspondence should be addressed. e-mail: wangzy6@sustech.edu.cn; tel.: +86-075588018040;

Contents

1. Supplementary Experimental Section

Text S1 Chemical reagents

Text S2 Preparation of single-layer MoS₂ nanosheets

Text S3 Fractal dimension analysis by static light scattering

Text S4 Normalized number of nanoclusters

Text S5 Adsorption isotherms

Text S6 Calculation of vdW attractions

2. Supplementary Figures and Tables

Figure S1 Conceptual model of (a) 1T- and (b) 2H-phase MoS₂

Figure S2 Linear relationship between MoS₂ concentration and DLS photon count rate

Figure S3 Increase in hydrodynamic diameter (D_h) for phase-transformed SL-MoS₂

Figure S4 Zeta potentials of SL-pristine as a function of cation concentrations

Figure S5 XPS Spectra of Mo 3d Pb 4f spectra

Figure S6 Attachment efficiencies of SL-MoS₂ as a function of Na⁺ concentration

Figure S7 XPS and Raman Characterization of FL-2H

Figure S8 Increase in hydrodynamic diameter (D_h) for SL-2H and FL-2H dispersions

Figure S9 vdW energies of nanoparticles and nanosheets

Figure S10 Increase in hydrodynamic diameter (D_h) at different MoS₂ mass concentrations

Figure S11 Water contact angles of MoS₂ membrane with different phase compositions.

Figure S12 Photographic images of SL-pristine and SL-2H redispersion after ultrasonification

Figure S13 The retained amount of MoS₂ in different positions of the column

Figure S14 Images of SEM characterization of retained MoS₂ in the sand column

Table S1 Freundlich and Langmuir model fitting parameters

1. Supplementary Experimental Section

Text S1 Chemical Regents. Ammonium molybdate tetrahydrate ($(\text{NH}_4)_6\text{Mo}_7\text{O}_{24}\cdot 4\text{H}_2\text{O}$, $\geq 99.9\%$), thioacetamide ($(\text{CH}_2\text{CSNH}_2)$, $\geq 99.9\%$) and hydrogen peroxide (H_2O_2 , 30%) were purchased from Macklin. Molybdenum disulfide powder (MoS_2 , $\geq 99.9\%$), *n*-Butyllithium and hexane solution were purchased from Sigma-Aldrich. The concentrated hydrochloric acid (HCl, 38%) was purchased from Lingfeng company and the sodium hydroxide (NaOH, 96%) was purchased from Shanghai Huagong. Diluted HCl and NaOH aqueous solutions were used to adjust pH. Solutions of Na^+ , Ca^{2+} , Mg^{2+} and Pb^{2+} were prepared from the sodium nitrate ($\text{Na}(\text{NO}_3)$, $\geq 99.9\%$), calcium nitrate tetrahydrate ($\text{Ca}(\text{NO}_3)_2\cdot 4\text{H}_2\text{O}$, $\geq 99.9\%$), magnesium nitrate hexahydrate ($\text{Mg}(\text{NO}_3)_2\cdot 6\text{H}_2\text{O}$, $\geq 99.9\%$) and lead nitrate ($\text{Pb}(\text{NO}_3)_2$, $\geq 99.9\%$), respectively, which were purchased from Sigma-Aldrich. Lead (II) and molybdenum (VI) standard solutions (1000 mg/L) were provided by Aladdin. The Milli-Q ultrapure water used in the experiment was produced by a purification system (resistivity $>18.2 \text{ M}\Omega\cdot\text{cm}$, Millipore, Billerica, MA).

Text S2 Preparation of Single-layer MoS_2 Nanosheets. To prepare chemically exfoliated single-layer MoS_2 (SL- MoS_2) nanosheets, a mixture of 300 mg MoS_2 powder in 3 mL of 1.6 M *n*-butyllithium was stirred for 48 h in a nitrogen-filled glovebox.¹ The resulting lithium-intercalated product was rinsed with 30 mL hexane twice to remove extra reagent and byproducts, followed by 60-min ultrasonication-assisted exfoliation in ultrapure water. Dispersion of SL- MoS_2 can be obtained by collecting the supernatant after centrifugation (15 min, 9,000 g). The final SL- MoS_2 dispersion was subjected to dialysis against water for 48 h to remove the byproduct LiOH and then stored in the glove box for maximum duration of 6 months until use.

Text S3 Fractal Dimension Analysis by Static Light Scattering. To obtain the fractal dimension of nanosheets' aggregates, scattering intensities at various detector angles were measured on a Wyatt DAWN HELEOS II MALS detector and analyzed as reported in prior studies.^{2,3} Briefly, the aggregates formed from the nanosheet dispersion (10 mg/L) were sampled after addition of 2 mM Ca²⁺ at 2 h, when the aggregates were visible. To study the structure of the aggregates, the intensity of scattered light I was measured at angles ranging from 20° to 120° for 5 s at each angle (corresponding to a series of scattering vector q). The structure information, quoted as the fractal dimension d_f , was obtained by plotting $\ln(I)$ vs $\ln(q)$. The slope of this plot is known as the scattering exponent and can be related to the d_f , which reveals the compactness of the aggregates.

Text S4 Normalized Number of Nanoclusters. The concentration of MoS₂ shows a good linear relationship ($R^2 > 0.99$) with the photon count rate of DLS (Figure S1). The normalized number of nanoclusters was obtained by using the number concentration at time t dividing the initial number concentration at $t = 0$ (N_t/N_0). Based on the Rayleigh scattering relationship, the ratio could use the photon count rate as an indicator of the number concentration as described:

$$\frac{N_t}{N_0} = \frac{P_t d_0^6}{P_0 d_t^6}$$

where P is the photon count rate (kcps), and d is the diameter of the nanoclusters. To ensure the average diameters of nanoclusters below the wavelength (638 nm) of the incident light, diluted MoS₂ suspension (2 mg/L) was employed to avoid rapid formation of large aggregates.

Text S5 Adsorption isotherms. Freundlich and Langmuir models were used to fit the adsorption isotherms. The Freundlich equation is an empirical model based on the multi-layer adsorption onto a heterogeneous surface, which is described as:

$$Q_e = K_f C_e^N$$

where Q_e (mg/g) is the adsorption density, K_f is the Freundlich affinity coefficient, N is the exponential coefficient, and C_e (mg/L) is the equilibrium concentration of the adsorbate. The Langmuir equation model assumes that the adsorption is a monolayer coverage on the adsorbent surface, which is described as follows:

$$Q_e = \frac{Q_m C_e K_L}{1 + K_L C_e}$$

where Q_m (mg/g) is the maximum adsorption capacity of the adsorbent and K_L is Langmuir constant.

Text S6 Calculation of vdW attractions. To explain the distinct aggregation behavior of nanosheets and nanoflowers, the vdW energy (W) between MoS₂ in different geometries was calculated using the models of interaction between two spheres (eq. 1) and two flat surfaces (eq. 2), respectively:⁴

$$W = \frac{-H R_1 R_2}{6D R_1 + R_2} \quad (1)$$

$$W = \frac{-HA}{12\pi D^2} \quad (2)$$

where H is the Hamaker constant of MoS₂, R is the radius of MoS₂ nanoparticles with $R_1=R_2=100$ nm, D is the distance between approaching nanomaterials and A is the area of the nanosheets (100×200 nm²).

2. Supplementary Figures

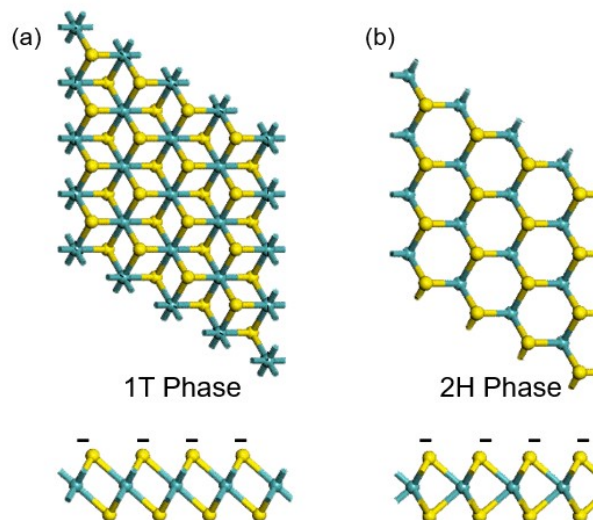


Figure S1. Conceptual model of (a) 1T- and (b) 2H-phase MoS₂ in top-down and cross-section views (balls in yellow and cyan represent S and Mo atoms, respectively).

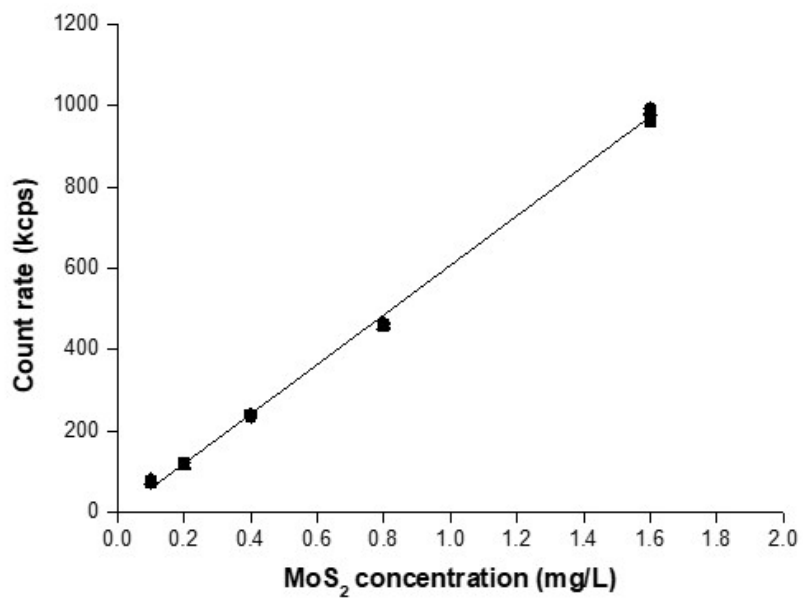


Figure S2. Linear relationship between MoS₂ concentration and DLS photon count rate.

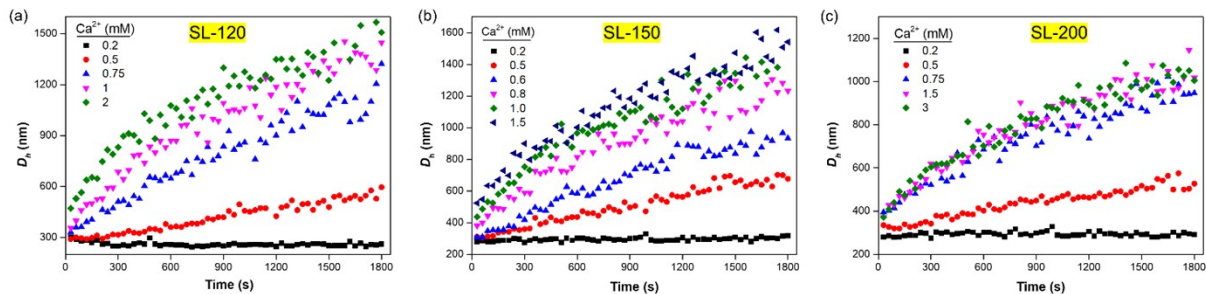


Figure S3. Increase in hydrodynamic diameter (D_h) for phase-transformed SL-MoS₂ over 30 min in the presence of the indicated amounts of Ca²⁺: (a) SL-120, (b) SL-150 and (c) SL-200.

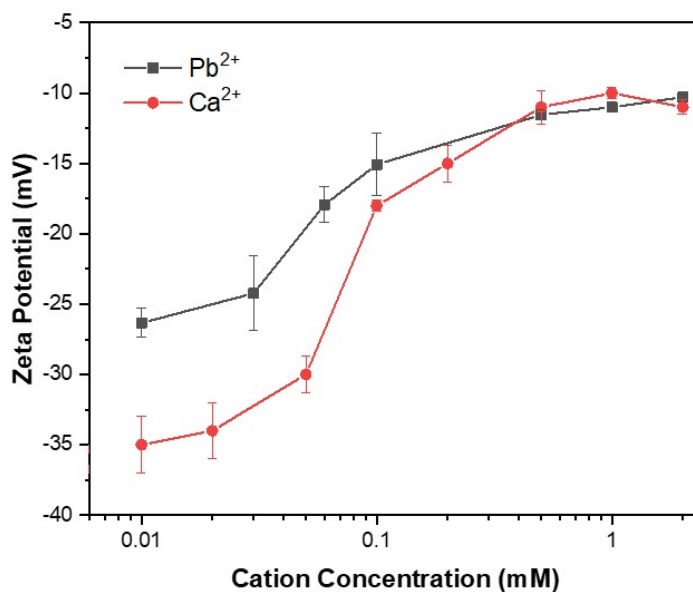


Figure S4. Zeta potentials of SL-pristine as a function of cation concentrations.

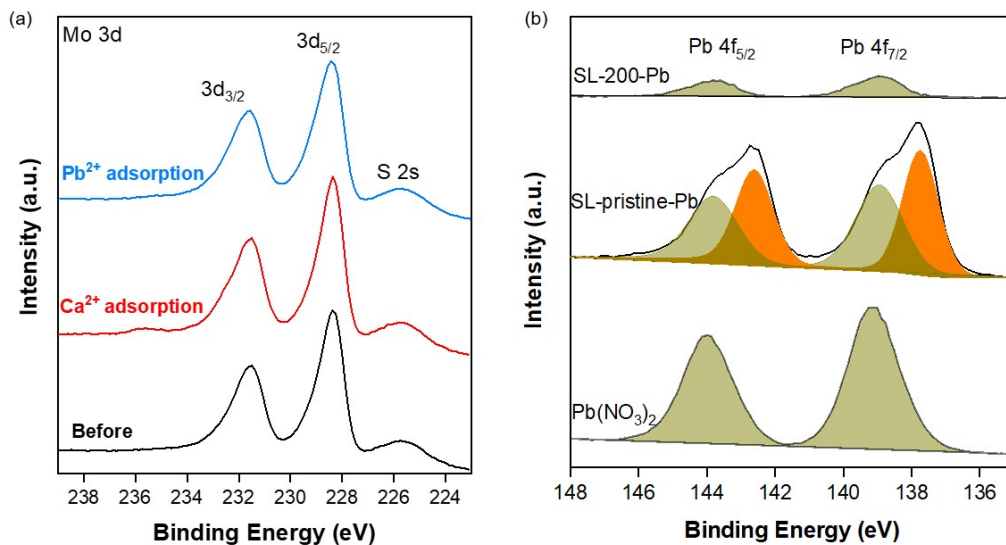


Figure S5. XPS Spectra of (a) Mo 3d of SL-pristine before and after Pb^{2+} or Ca^{2+} adsorption and (b) Pb 4f spectra before ($\text{Pb}(\text{NO}_3)_2$) and after Pb adsorption on SL-pristine and SL-200.

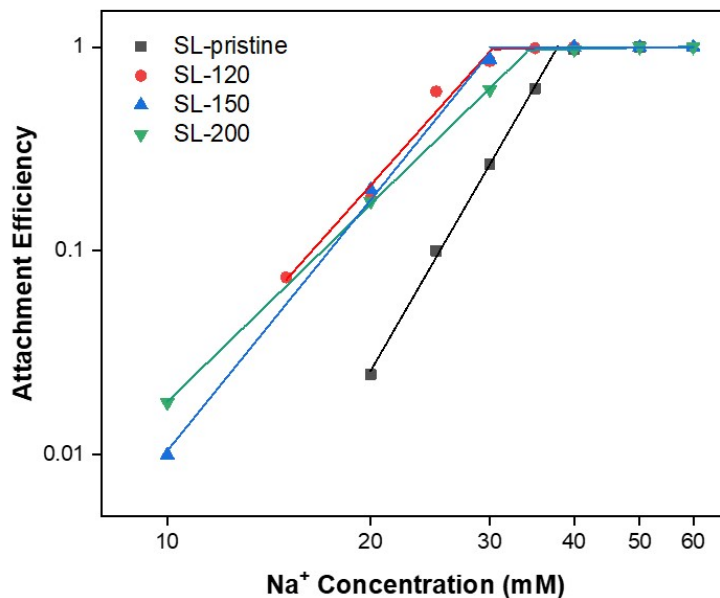


Figure S6. Attachment efficiencies of SL-MoS₂ with different phase composition as a function of Na⁺ concentration.

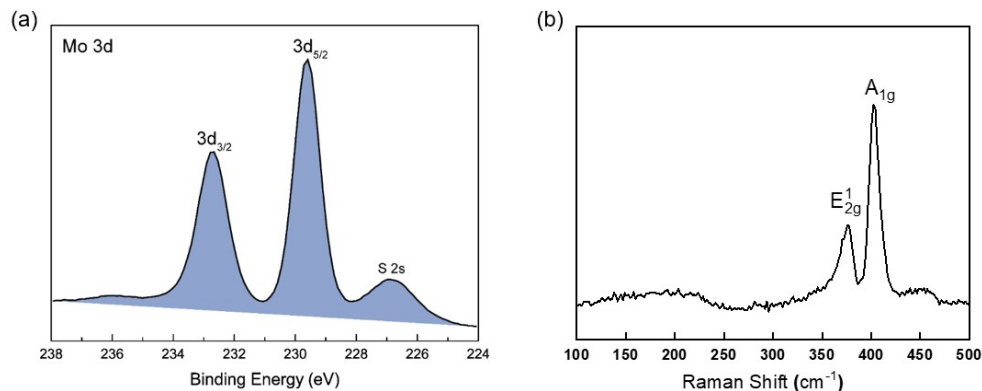


Figure S7. Characterization of FL-2H: (a) XPS spectra and deconvolution analysis of Mo and (b) Raman spectra, showing the only component of semiconducting 2H phase in flower-like MoS₂ nanoparticles.

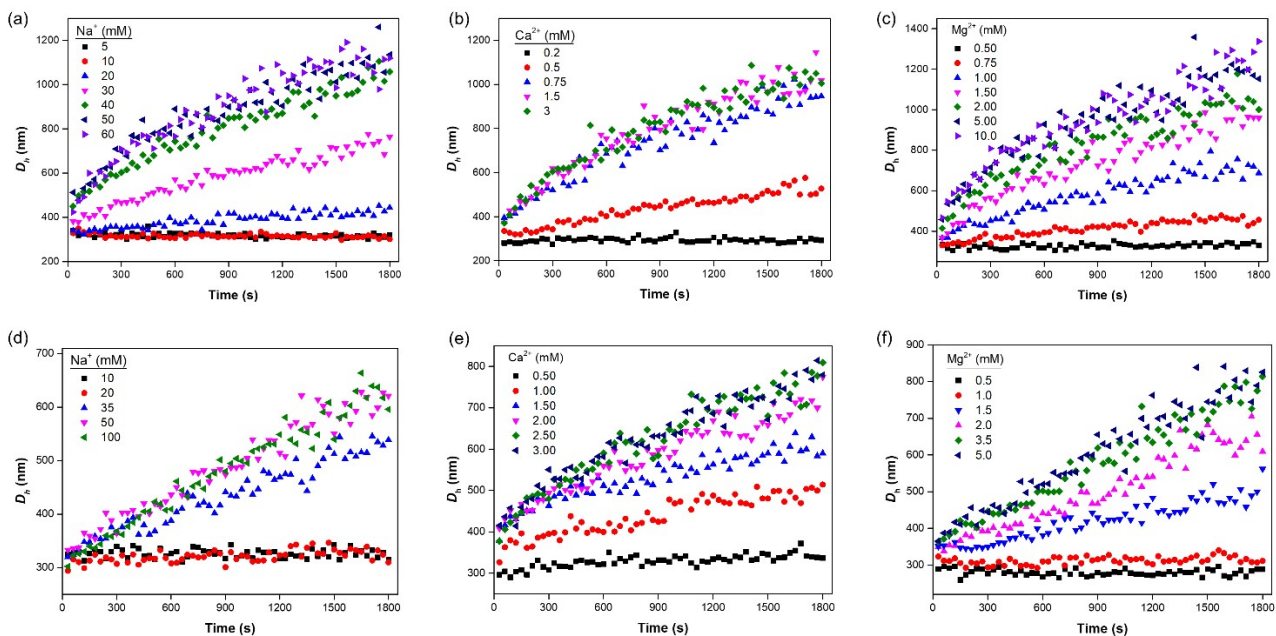


Figure S8. Increase in hydrodynamic diameter (D_h) for SL-2H (a–c) and FL-2H (d–f) dispersions over 30 min in the presence of the indicated cations.

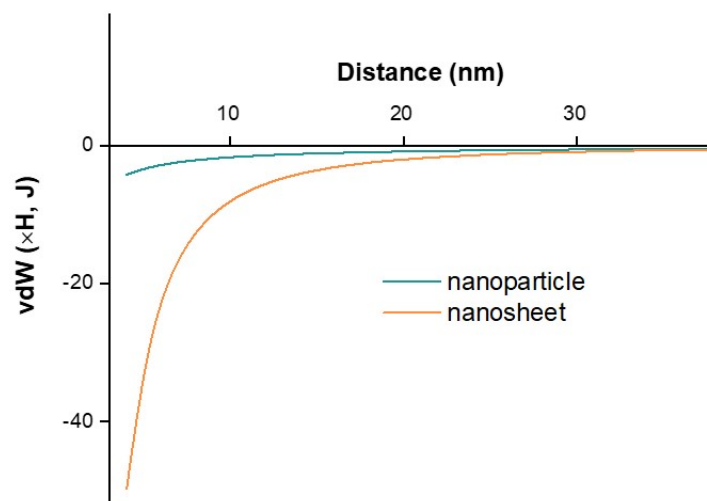


Figure S9. vdW energies of nanoparticles and nanosheets as calculated by sphere-sphere and surface-surface model, respectively.

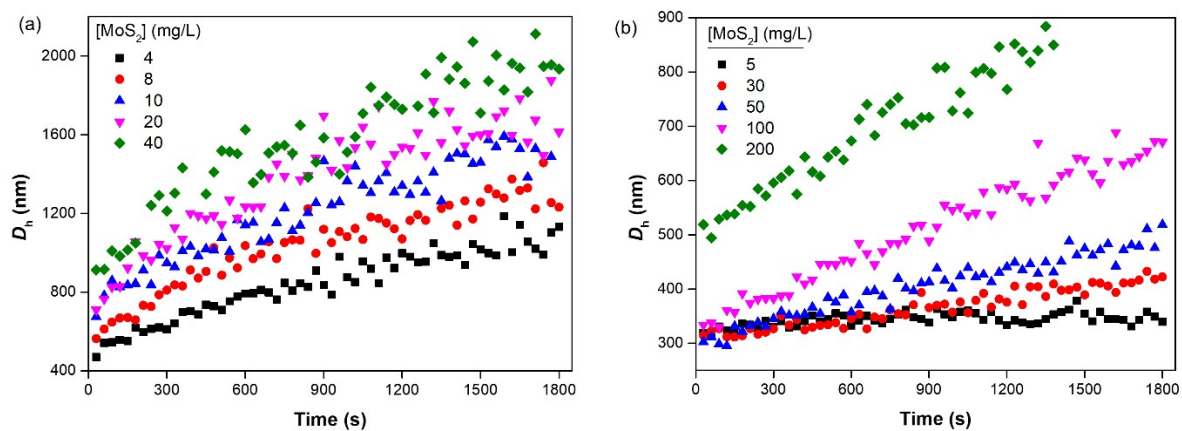


Figure S10. Increase in hydrodynamic diameter (D_h) at different MoS_2 mass concentrations: (a) SL-2H and (b) FL-2H.

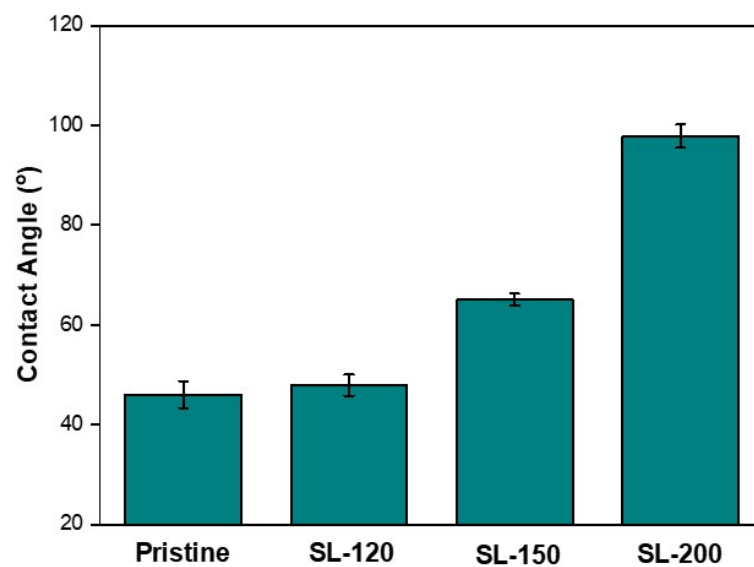


Figure S11. Water contact angles of MoS₂ membrane prepared from nanosheets with different phase compositions.

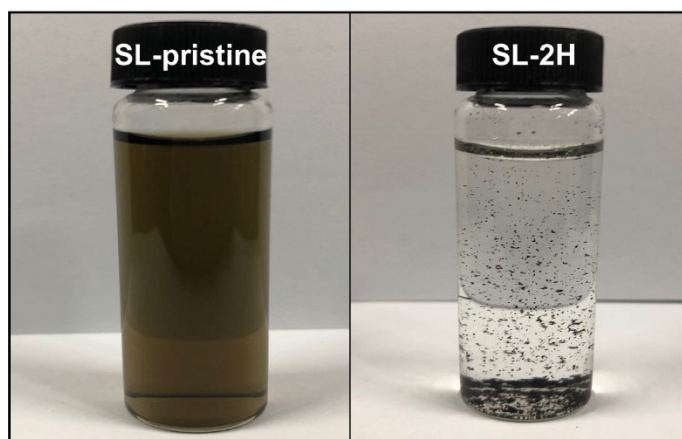


Figure S12. Photographic images of SL-pristine and SL-2H redispersion after ultrasonification.

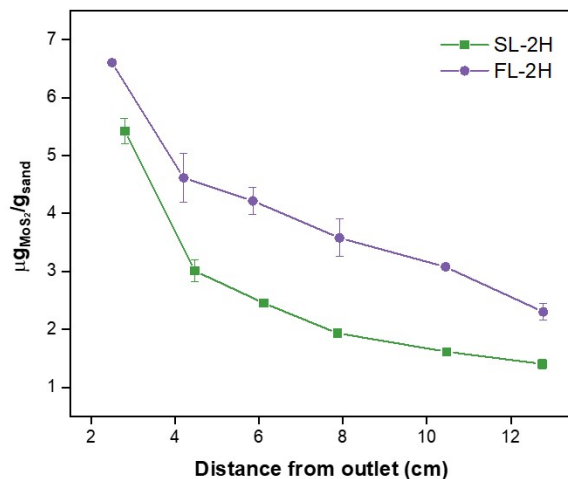


Figure S13. The retained amount of MoS_2 in different positions of the column.

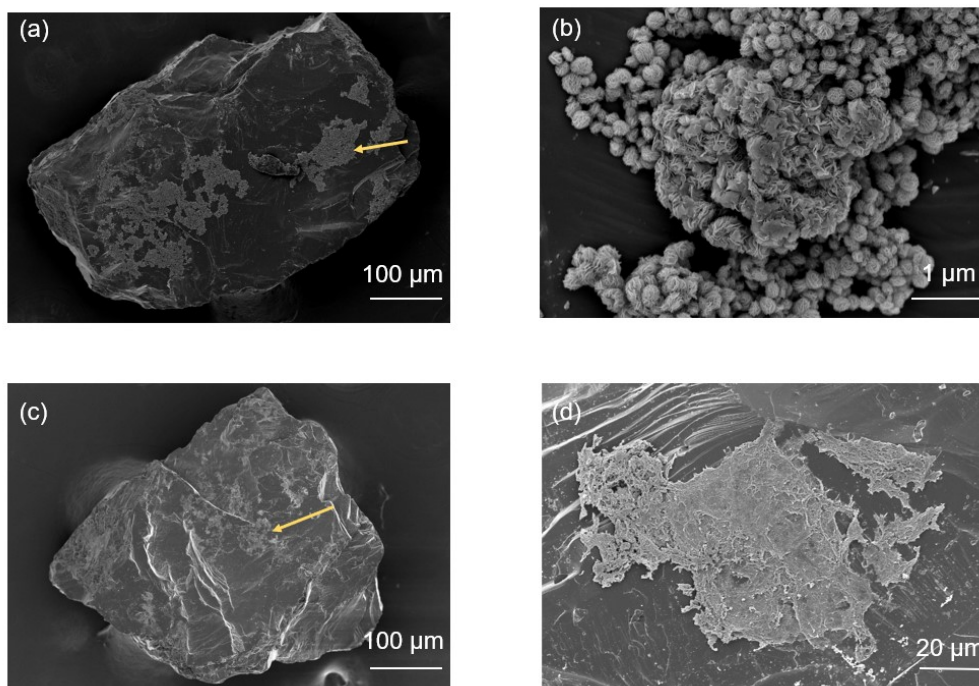


Figure S14. Images of SEM characterization of retained MoS_2 in the sand column: (a) FL-2H on the sand, (b) magnified image for the area marked by arrow in a; (c) SL-2H on the sand and (d) magnified image for the area marked by arrow in b.

Table S1. Freundlich and Langmuir model fitting parameters (mean \pm error) of the Pb²⁺ adsorption isotherm on pristine and transformed SL-MoS₂.

Models	Freundlich			Langmuir		
	K_f	N	R^2	Q_m	K_L	R^2
SL-pristine	451.1 \pm 44	0.149 \pm 0.03	0.88	699.2 \pm 30	34.3 \pm 12	0.95
SL-120	461.8 \pm 25	0.078 \pm 0.02	0.86	564.3 \pm 20	533.9 \pm 209	0.90
SL-150	286.5 \pm 38	0.117 \pm 0.03	0.87	388.1 \pm 30	37.6 \pm 29	0.92
SL-200	245.8 \pm 21	0.11 \pm 0.02	0.82	339.2 \pm 9	41.3 \pm 11	0.96

References

- 1 Z. Wang, A. Von Dem Bussche, Y. Qiu, T. M. Valentin, K. Gion, A. B. Kane and R. H. Hurt, Chemical Dissolution Pathways of MoS₂ Nanosheets in Biological and Environmental Media, *Environ. Sci. Technol.*, 2016, **50**, 7208–7217.
- 2 Z. Li, S. Shakiba, N. Deng, J. Chen, S. M. Louie and Y. Hu, Natural Organic Matter (NOM) Imparts Molecular-Weight-Dependent Steric Stabilization or Electrostatic Destabilization to Ferrihydrite Nanoparticles, *Environ. Sci. Technol.*, 2020, **54**, 6761–6770.
- 3 R. Amal, J. A. Raper and T. D. Waite, Effect of fulvic acid adsorption on the aggregation kinetics and structure of hematite particles, *J. Colloid Interface Sci.*, 1992, **151**, 244–257.
- 4 J. N. Israelachvili, *Van der Waals Forces between Particles and Surfaces*, Academic press, Waltham, MA, 2011.